Improved, Robust, Axial Line Singularity Method for Bodies of Revolution

Michael J. Hemsch*
PRC Aerospace Technologies Division, Hampton, Virginia

The axial line singularity method has been a popular engineering approach for representing incompressible, inviscid flow about an inclined slender body of revolution since von Kármán first used it more than 60 years ago. Despite its usefulness, however, practitioners have been plagued by failures of the method for many bodies of practical interest. Various approaches have been developed for increasing the range of applicability of the method but none of them can be counted on to work in general. The present paper points out that the source of the failures is common to all attempts to solve Fredholm equations of the first kind and shows that a previously developed smoothing technique yields a robust method for numerically solving the governing equations. The technique is easily retrofitted to existing codes and requires very little extra computational work. The method allows the number of singularities to be increased until the most accurate line singularity solution is obtained. The technique is applied to various difficult bodies and comparisons with data are given.

Nomenclature

A_j = quadrature weight for jth node
a = location of forward end of singularity distribution
b = location of aft end of singularity distribution; also parameter in description of test-case body
C = smoothing matrix
c_n = see Eq. (17)
c_p = pressure coefficient
d_n = see Eq. (18)
$F(x)$ = function describing body surface [see Eq.(3)]
f = unknown singularity strength vector
g = known right side vector
$K_1(x,x')$ = kernel for source distribution
$K_2(x,x')$ = kernel for doublet distribution
$\hat{K}$ = coefficient matrix, [see Eq.(25)]
$\hat{K}^T$ = transpose of $\hat{K}$
L = body length
L_n = forebody length
M = number of conditions
M_∞ = freestream Mach number
N = number of nodes
q = source singularity strength
$R(x)$ = body radius at axial station x
$S(x)$ = cross-sectional area distribution normalized by maximum value
U_∞ = freestream velocity
V = flow velocity
V_n = component of flow velocity normal to body surface
x,r,θ = cylindrical coordinates aligned with body axis with origin at nose tip and with θ measured from the windward meridian
α = angle of attack
γ = smoothing parameter
ϵ = R_{max}/L
μ = doublet singularity strength
ξ = axial distance from singularity
ρ = ratio of ith interval length to i-1th interval length
Φ = velocity potential [see Eq.(1)]
ϕ_1 = velocity potential for axial-flow problem
ϕ_2 = velocity potential for cross-flow problem

Subscripts

s = shoulder
1 = source (axial) problem
2 = doublet (crossflow) problem

Presented as Paper 89-2176 at the AIAA 7th Applied Aerodynamics Conference, Seattle, WA, July 31-Aug. 2, 1989; received Aug. 26, 1989; revision received Dec. 12, 1989.

*Engineering Specialist; currently with Lockheed Engineering & Sciences Company, Hampton, VA. Associate Fellow AIAA.

Introduction

VON Kármán[1] was apparently the first to use the axial line singularity method to represent an arbitrary slender body of revolution in inviscid, incompressible flow. Since then many workers have used it to solve a variety of problems of practical interest. The method reduces the governing partial differential equation (Laplace) and the boundary conditions to two uncoupled Fredholm equations of the first kind, which have been solved by a variety of approaches including direct iteration,[2,3] uniform asymptotic expansions,[4-7] a hybrid perturbation Galerkin method,[2] and the method of undetermined coefficients.[8] The method most favored by engineers is numerical integration and collocation (NIC),[1,9-24] apparently because of its greater generality and ease of use.

It is well known that the coefficient matrix for the system of linear equations produced by the NIC method is ill conditioned[10,16-20] and often produces solutions with unacceptable oscillations when improved accuracy is attempted by increasing the number of singularities. To reduce the effects produced by attempting to invert the ill-conditioned matrix, workers have resorted to using a double precision,[16-20] least-squares solution of an overdetermined system[19,20,22,23] and optimization of the location of the singularities.[22-24] Despite all of the preceding efforts, no robust method has been developed.

In this paper, it is shown that a numerical technique developed for solution of remote sensing problems[25,26] can be applied to the NIC method, and that it produces good solutions for bodies previously considered too difficult for the method. Very little extra programming effort or central processing unit (CPU) time is required. Because the method is robust, it is now possible to increase the number of singularities until the most accurate line singularity solution has been obtained for the machine roundoff error used.

The next section describes the standard reduction of the governing differential equation and the boundary conditions

to two uncoupled Fredholm equations of the first kind. In the following section, the importance of correctly choosing the extent of the axial singularity distributions for each body of interest is discussed, and formulas derived elsewhere for estimating that extent are presented. The smoothing algorithm used in the present study is given next, and a test case is used to illustrate the behavior of the NIC method with and without smoothing. Following that section, solutions are presented for four difficult example cases and compared with experimental data.

Reduction to Fredholm Equations of the First Kind

A velocity potential for inviscid, incompressible flow is defined such that

$$V = U_\infty + \nabla\Phi \tag{1}$$

where $\Phi \to 0$ as $r \to \infty$. The potential is governed by Laplace's equation which, in cylindrical coordinates, is given by

$$\Phi_{rr} + \Phi_r/r + \Phi_{\theta\theta}/r^2 + \Phi_{xx} = 0 \tag{2}$$

The boundary condition is

$$V \cdot \nabla F = 0 \tag{3}$$

where $F(r,x) = r - R(x) = 0$ describes the body surface.

Because Eq. (2) is linear and the bodies of interest are axisymmetric, the three-dimensional flow problem can be split into two two-dimensional, axisymmetric problems: one at 0 deg and the other at 90 deg angle of attack. The freestream velocity for both is unity. The potentials for the two split problems, ϕ_1 and ϕ_2, respectively, are defined by

$$\Phi(x,r,\theta) = U_\infty[\phi_1(x,r)\cos\alpha + \phi_2(x,r)\sin\alpha\cos\theta] \tag{4}$$

where θ is measured from the windward meridian. Substituting Eq. (4) into Eq. (2) and separating terms gives the following governing equations for ϕ_1 and ϕ_2:

$$\phi_{1rr} + \phi_{1r}/r + \phi_{1xx} = 0 \tag{5}$$

$$\phi_{2rr} + \phi_{2r}/r + \phi_{2xx} - \phi_2/r^2 = 0 \tag{6}$$

Substituting Eq. (4) into Eq. (3) and separating terms gives the following boundary conditions for ϕ_1 and ϕ_2:

$$\phi_{1r} = (1 + \phi_{1x})\,dR/dx \tag{7}$$

$$\phi_{2r} = (1 + \phi_{2x})\,dR/dx \tag{8}$$

The following elementary source and doublet solutions will be used for ϕ_1 and ϕ_2, respectively:

$$\phi_1 = -1/[4\pi(r^2 + \xi^2)^{1/2}] \tag{9}$$

$$\phi_2 = -r/[4\pi(r^2 + \xi^2)^{3/2}] \tag{10}$$

where ξ is the axial distance from the discrete singularity. Distributing the above singularities continuously on the axis of the body and summing gives

$$\phi_1(x,r) = -\frac{1}{4\pi}\int_{a_1}^{b_1} \frac{q(x')\,dx'}{[r^2 + (x-x')^2]^{1/2}} \tag{11}$$

$$\phi_2(x,r) = -\frac{r}{4\pi}\int_{a_2}^{b_2} \frac{\mu(x')\,dx'}{[r^2 + (x-x')^2]^{3/2}} \tag{12}$$

The proper values for the limits of the distributions (i.e., a and b) will be discussed in the next section.

Differentiating Eqs. (11) and (12) with respect to x and r, evaluating the results on the body, and substituting those results into Eqs. (7) and (8) gives

$$\int_{a_1}^{b_1} K_1(x,x')q(x')\,dx' = 4\pi\,dR/dx \tag{13}$$

$$\int_{a_2}^{b_2} K_2(x,x')\mu(x')\,dx' = 4\pi \tag{14}$$

where the kernel functions $K_1(x,x')$ and $K_2(x,x')$ are given by

$$K_1(x,x') = [R - (x-x')\,dR/dx][R^2 + (x-x')^2]^{-3/2} \tag{15}$$

$$K_2(x,x') = -[R^2 + (x-x')^2]^{-3/2} + 3R[R - (x-x')\,dR/dx][R^2 + (x-x')^2]^{-5/2} \tag{16}$$

Equations (13) and (14) are the Fredholm equations of the first kind used in the NIC method.

Domain of the Singularity Distributions

It has been established that the choice of limits for the source and doublet distributions on the body axis can have a significant effect on the accuracy and reliability of the NIC method (e.g., see Refs. 3 and 13). Fortunately, workers using uniform asymptotic expansions have determined those limits precisely for bodies whose cross-sectional area distributions can be expanded about the stagnation points in power series that converge over the entire length of the body; i.e., $S(x)$ is analytic. In this paper, those limits will be used even when the cross-sectional area distribution of the body of interest is not analytic.

Although Lotz[27] was apparently the first to note the importance of correctly fixing the extent of the singularity distributions, Moran[4] appears to have been the first to show formally that the size of the gaps between the ends of the source distribution and the body end points could be determined precisely by requiring that successive approximations be uniformly valid. Handelsman and Keller[5] achieved the same results using a somewhat different technique. Handelsman and Keller's results are now presented.

$S(x)$ is normalized such that $S_{\max}$ is unity and all dimensions are normalized by the body length. It is further assumed that $S(x)$ is analytic on $0 \le x \le 1$ with $S(0) = S(1) = 0$ and can be expanded in power series about the end points as follows:

$$S(x) = \sum_{n=1}^{\infty} c_n x^n \tag{17}$$

where $c_n = S^{(n)}(0)/n!$ and

$$S(x) = \sum_{n=1}^{\infty} d_n (1-x)^n \tag{18}$$

where $d_n = (-1)^n S^{(n)}(1)/n!$. The locations of the ends of the source density distribution are then given by

$$a_1 = (\epsilon/2)^2 c_1[1 - c_2(\epsilon/2)^2 + (c_1c_3 + 2c_2^2)(\epsilon/2)^4 - (c_1^2c_4 + 7c_1c_2c_3 + 5c_2^3)(\epsilon/2)^6] + \mathcal{O}(\epsilon^{10}) \tag{19}$$

$$b_1 = 1 - (\epsilon/2)^2 d_1[1 - d_2(\epsilon/2)^2 + (d_1d_3 + 2d_2^2)(\epsilon/2)^4 - (d_1^2d_4 + 7d_1d_2d_3 + 5d_2^3)(\epsilon/2)^6] + \mathcal{O}(\epsilon^{10}) \tag{20}$$

where ϵ is the ratio of the maximum radius to the body length.

It is easy to show from Handelsman and Keller's[5] results that the first terms of Eqs. (19) and (20) correspond to placing the ends of the distribution at inset distances of one-half the radii of curvature of the body end points. This value was suggested by Thwaites[3] and Shu and Kuhlman.[13-15]

By applying the method[5] of Handelsman and Keller to the crossflow problem, Geer[6] was able to show that the doublet distribution must have the same extent as the source distribu-

tion. Hence,

$$a_2 = a_1 = a \tag{21}$$

$$b_2 = b_1 = b \tag{22}$$

Geer further showed that the doublet strength at the limits of the distribution must be zero.[6] Note that for a pointed tip the inset distance is zero. It is easy to show that the source strength at a pointed tip must also be zero.

Numerical Integration and Collocation Method and Smoothing

Twomey's Algorithm

It has become standard practice to solve Eqs. (13) and (14) numerically by assuming piecewise linear variations for q and μ, carrying out the quadratures and inverting the resulting linear system of equations. Unfortunately, as pointed out by Dahlquist and Björck[28] and Phillips,[25] an ill-conditioned system can be expected because of machine roundoff error. In fact, Phillips showed that, for any Fredholm equation of the first kind with a smooth kernel, as the mesh width (distance between nodes of the distribution) decreases, the solutions at first become more accurate, but eventually begin to get worse. How soon the solutions begin to get worse depends on the roundoff error, which explains the partial success workers have had using double precision. Phillips also pointed out that the error in each of the approximate solutions tends to be an oscillatory function of x. This behavior can be seen in solutions in the literature (e.g., see Ref. 19).

In order to find acceptable solutions with the NIC method, Phillips[25] assumed that the unknown distribution is a reasonably smooth function and minimized the second differences in the resulting solution using the technique of Lagrange multipliers. In this paper Phillip's method will be applied in the improved version given by Twomey.[26]

Consider Eqs. (13) and (14) in the following generic form

$$\int_{a_1}^{b_1} K(x,x')f(x')\,dx' = g(x) \tag{23}$$

The NIC method consists of discretizing the integrand of Eq. (23), applying an appropriate quadrature formula, and evaluating the kernel and right side at a series of points on the body. Other conditions, such as requiring that the total source strength of a closed body be zero, may be included as well. Carrying out the discretization and collocation for Eq. (23) gives the following system of linear equations

$$\sum_{j=1}^{N} K(x_i,x_j)A_j f(x_j) = g(x_i), \qquad i = 1, 2, \ldots, M \tag{24}$$

where the A_j are the coefficients in the quadrature formula and $M \geq N$. In the present work, the singularity distributions are assumed to be piecewise linear, and quadratures are carried out between nodes on the axis to get the $K(x_i,x_j)A_j$ terms. It is convenient to define

$$\hat{K}(x_i,x_j) \equiv K(x_i,x_j)A_j \tag{25}$$

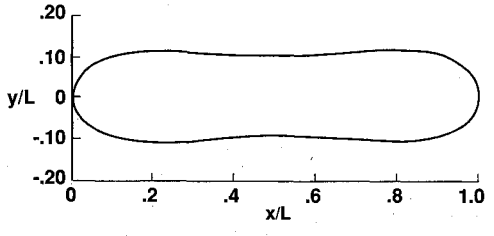

Fig. 1 Dumbbell shape for test case; $\epsilon = 0.11$, $b = 3$.

so that Eq. (24) is

$$\hat{K}f = g \tag{26}$$

Twomey's simplified version of Phillips' algorithm is given by[26]:

$$(\hat{K}^T\hat{K} + \gamma C)f = \hat{K}^T g \tag{27}$$

where γ is an arbitrary positive constant, and the second-differences smoothing matrix C is given by

$$C = \begin{bmatrix} 1 & -2 & 1 & 0 & 0 & \cdot & \cdot & \cdot \\ -2 & 5 & -4 & 1 & 0 & \cdot & \cdot & \cdot \\ 1 & -4 & 6 & -4 & 1 & 0 & \cdot & \cdot \\ 0 & 1 & -4 & 6 & -4 & 1 & 0 & \cdot \\ \cdot & \cdot & \cdot & \cdot & \cdot & \cdot & \cdot & \cdot \end{bmatrix} \tag{28}$$

There are several comments to be made about Eq. (27). First, note that an overdetermined system can be handled and, indeed, for $\gamma = 0$, Eq. (27) reduces to the least-squares form.[22,23,28] Second, very little extra work is needed to solve Eq. (27) compared to Eq. (26) since most of the work involved consists of filling $\hat{K}$ and inverting the coefficient matrix. Third, once the $\hat{K}^T\hat{K}$, C, and $\hat{K}^T g$ matrices are formed, multiple solutions for various values of γ can be obtained easily. This is an important point because the most accurate solution for a given distribution of nodes is usually given by the smallest value of γ for which an acceptably smooth solution is generated. The solutions appear to be very weak functions of γ. Consequently, working at a graphics terminal and varying γ by an order of magnitude at a time will produce the best solution in several minutes of real time on a superminicomputer such as the Gould PN9005 or VAX 780. All of the results presented in this paper were obtained using single precision on the Gould PN9005, which is a 32-bit machine.

For design codes that require batch processing, it will be shown later that smoothing values (γ) between 0.001 and 0.01 for the source solution and between 0.1 and 10 for the doublet solution should produce good results. However, the user should still monitor the maximum and rms values of the residual velocity component normal to the body surface.

Test Case

An analytic body previously investigated by Geer[2] and Wong et al.[7] has been chosen to illustrate the method. The dumbbell-like body is shown in Fig. 1 and is given by

$$R(x) = \epsilon\sqrt{S(x)} \tag{29}$$

where

$$S(x) = 4bx(1-x)[1 - bx(1-x)] \tag{30}$$

For this case, $\epsilon = 0.11$ and $b = 3$. Although the chosen body has a cross-sectional area distribution that is analytic and fairly benign looking, the solutions nicely illustrate the behavior described in the previous section.

In order to obtain satisfactory accuracy at the ends of the body, it was found necessary to cluster nodes near the inset points. Consequently, exponential stretching was used to set up the location of the nodes between the inset distance for each end of the body and the midpoint. For example, the node locations for the front half of the body are given by

$$x_i = a + (1-\rho^i)(L/2 - a)/(1-\rho^{N-1}) \tag{31}$$

where $\rho = x_{i+1}/x_i$, and good results are usually found for values between 1.02 and 1.15.

The boundary conditions given by Eqs. (7) and (8) were applied at the interval midpoints, at the body midpoint, and at the midpoints of the inset gaps. For the source (axial) solu-

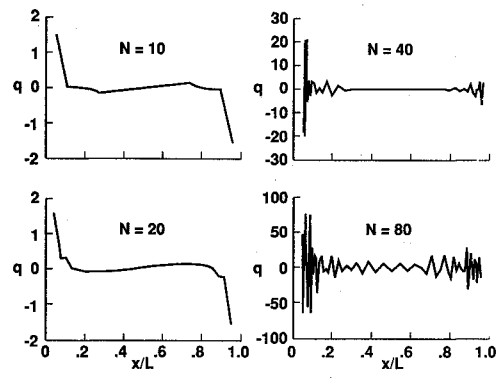

a) Source strength

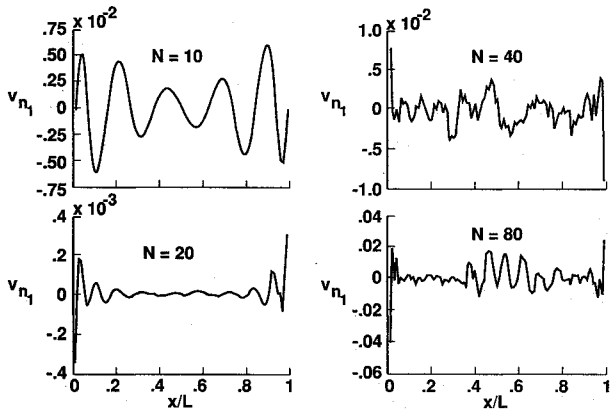

b) Component of velocity normal to body surface

Fig. 2 Axial flow solutions for dumbbell test case; $\gamma_1 = 0$.

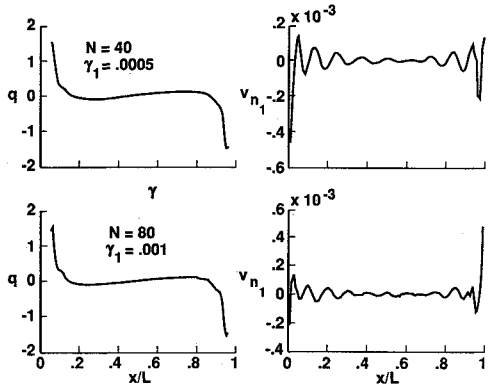

a) Source strength and normal velocity distributions

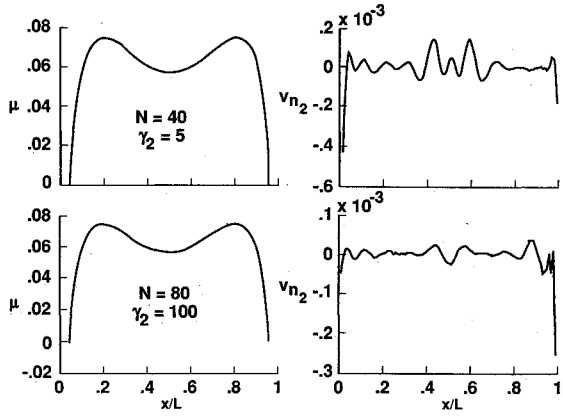

b) Doublet strength and normal velocity distributions

Fig. 4 Smoothed solutions for dumbbell test case.

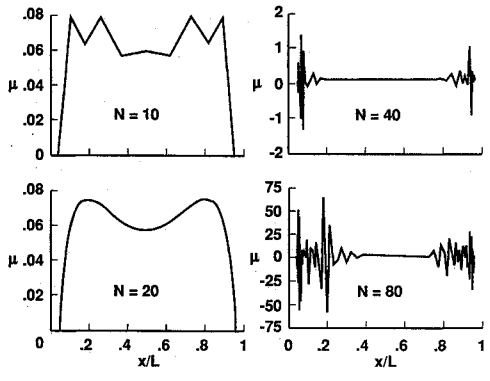

a) Doublet strength

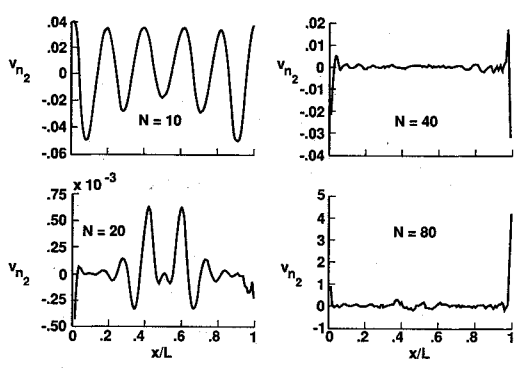

b) Component of velocity normal to body surface

Fig. 3 Crossflow solutions for dumbbell test case; $\gamma_2 = 0$.

tions, the additional conditions of stagnation at the ends of the body, and a total source strength of zero were also applied. Consequently, the number of conditions for the source and doublet solutions were $N + 5$ and $N + 2$, respectively.

The source solutions for no smoothing are given in Fig. 2a for $N = 10$, 20, 40, and 80. A measure of the accuracy of the solutions is given by the component of velocity normal to the surface as given in Fig. 2b. Note the different vertical scales. As predicted by Phillips,[25] the solution does improve for $N = 20$ but deteriorates badly as N is increased further. Similar results for the doublet solution are given in Fig. 3.

Smoothed source and doublet solutions for $N = 40$ and 80 are given in Fig. 4. The smoothing values used are shown in the figure. The source results show that increasing N beyond a value of 20 improves the error only slightly. However, the error improvement obtained in the doublet solution by increasing N to 40 and 80 is obvious (compare with Fig. 3b). Note that, for this case, γ_2 is four to five orders of magnitude larger than γ_1.

Pressure distributions along the windward meridian for $N = 80$ are given in Fig. 5 for $\alpha = 0$ and 90 deg. Smoothed and unsmoothed solutions are given to demonstrate the need for using smoothing.

Applications

Tangent-Ogive-Cylinder-Boattail

In this section, the present method will be applied to four difficult configurations and the solutions compared with experiment. The boundary conditions are applied at the midpoints of the singularity intervals, and the distributions are allowed to be discontinuous at the forebody shoulder following the suggestion of Shu and Kuhlman.[13] The first two bodies were tested by Fox[29] and are shown in Fig. 6. The body at the top of the figure has a one-caliber tangent-ogive forebody, a two-caliber, cylindrical midsection, and a 0.5-caliber 10-deg

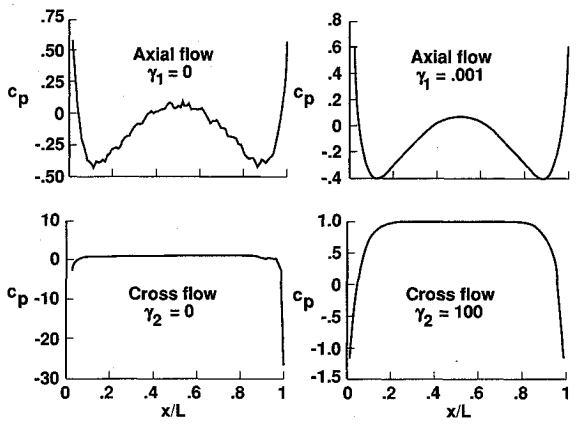

Fig. 5 Comparisons of pressure distributions along windward ray for unsmoothed and smoothed axial and crossflow solutions for $N = 80$.

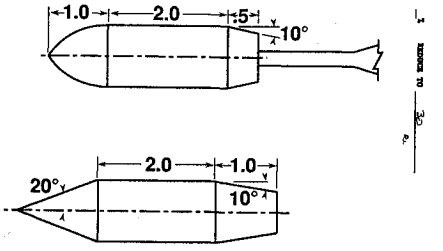

Fig. 6 Forebody-cylinder-boattail test cases[29] (all dimensions are normalized by the cylinder diameter).

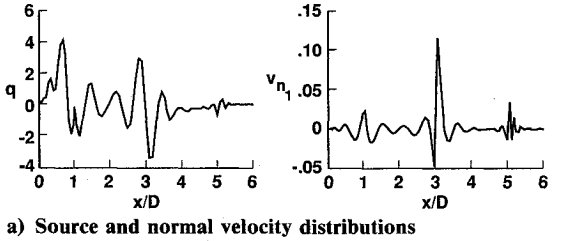

a) Source and normal velocity distributions

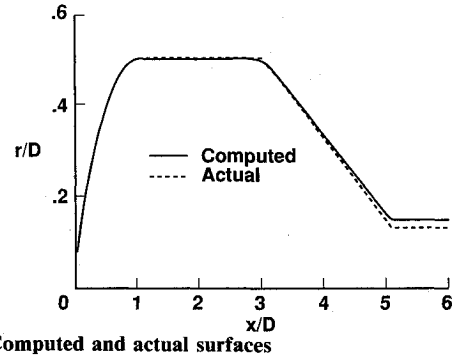

b) Computed and actual surfaces

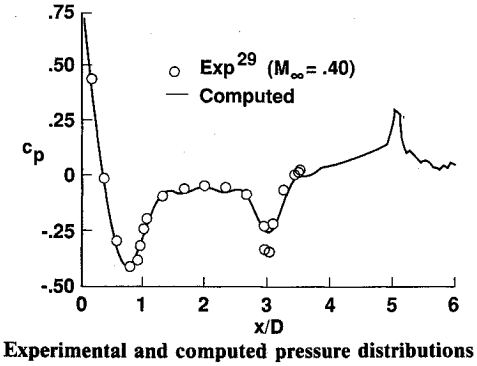

c) Experimental and computed pressure distributions

Fig. 7 Axial-flow solution for test configuration shown at top of Fig. 6; forebody is one-caliber tangent ogive.

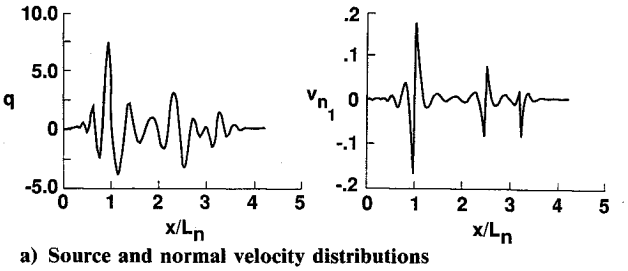

a) Source and normal velocity distributions

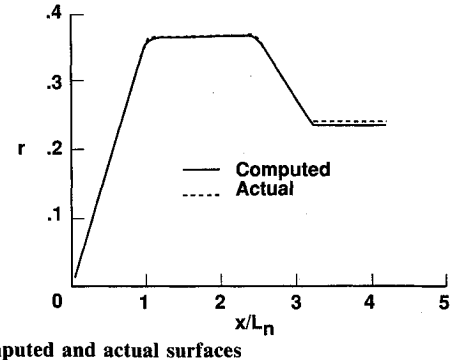

b) Computed and actual surfaces

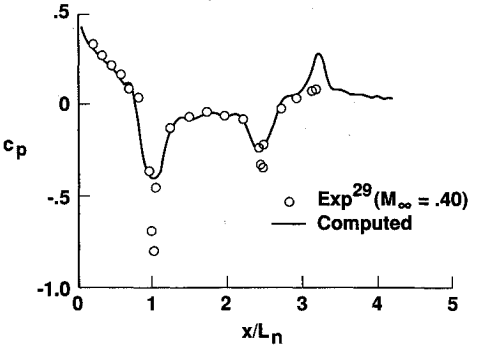

c) Experimental and computed pressure distributions

Fig. 8 Axial-flow solution for test configuration at bottom of Fig. 6; forebody is a 20-deg half-angle cone.

conical boattail. This case is interesting because of the very-low-fineness-ratio forebody (the tip half angle is 53 deg) and the discontinuous slope at the midsection-boattail shoulder. Since the line singularity method cannot handle a discontinuity in the body radius, the boattail was modeled as if it continued to the sting. It is assumed that the sting extends to infinity.

The axial flow solution for the preceding configuration is given in Fig. 7. 95 nodes were used to model the body-sting combination with 30 of them placed on the tangent-ogive forebody. The best value of γ_1 was found to be 0.01. Note that the largest errors in the normal velocity occur at the three shoulders where there are discontinuities in either the slope or the second derivative.

Since the errors shown in Fig. 7a are so large compared to those obtained for the smooth test body of Fig. 1, it is instructive to compare the model body with that actually computed. This can be done by solving the equation for the location of the streamline which goes through the nose tip

$$\pi R_\infty^2 = 2\pi R^2 - \int_a^b \frac{q(x')(x-x')\,dx'}{[R^2 + (x-x')^2]^{1/2}} \tag{32}$$

where $R(x)$ is the radial position of the streamline. Equation (32) must be solved by iteration. The result for the top model of Fig. 6 is given in Fig. 7b. Note the rounding of the shoulders with slope discontinuities and the slight undulations over the midsection and the boattail. The rounding and undulations appear to be inevitable for bodies with slope discontinuities. However, with the present smoothing technique, they can be controlled. Unfortunately, with very large slope discon-

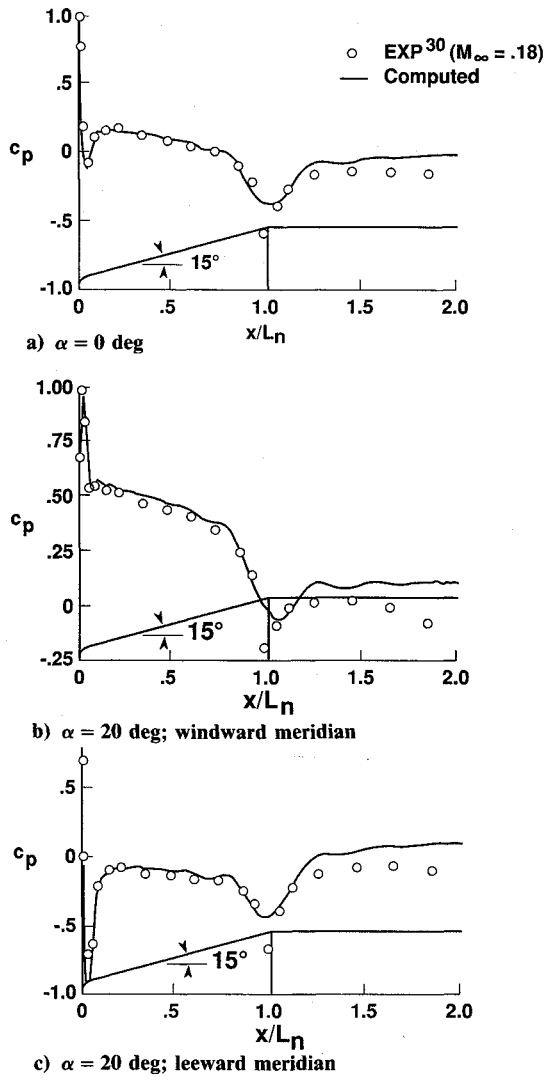

Fig. 9 Comparison of theory and experiment for 15-deg half-angle cone cylinder with 25% bluntness.

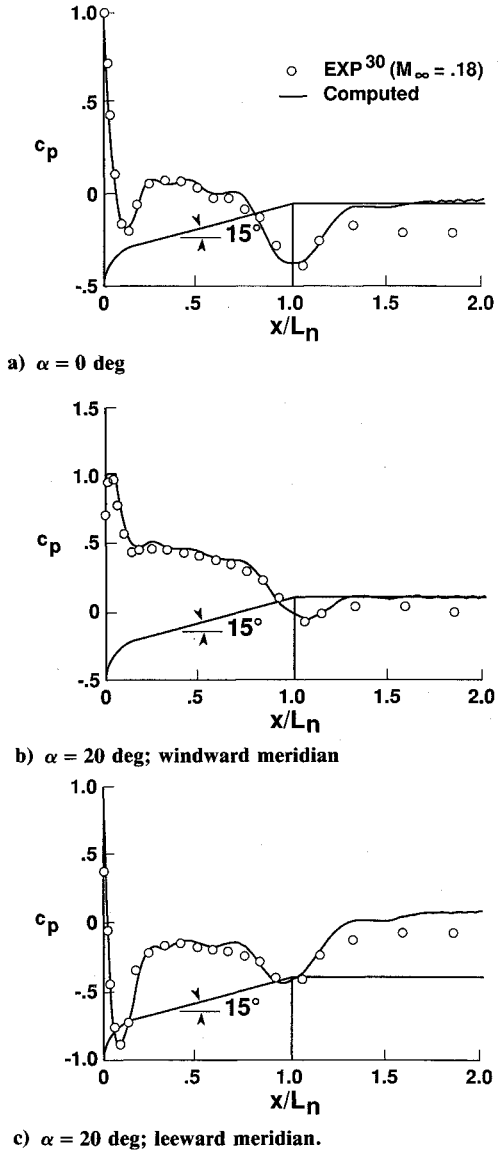

Fig. 10 Comparison of theory and experiment for 15 deg half-angle cone cylinder with 50% bluntness.

tinuities, reducing the undulations by increasing the value of the smoothing parameter results in more rounding of the shoulder even if local node clustering is used. A comparison of experimental[29] and computed pressures along a meridian for $\alpha = 0$ are given in Fig. 7c. The comparison is good for the forebody and midsections but the rounding of the midsection-boattail shoulder prevents simulation of the peak suction pressure.

20 deg Cone-Cylinder-Boattail

The second body is shown at the bottom of Fig. 6. It has the same sting as the top body. Wolfe and Oberkampf[17] found that a good representation of the 20 deg half-angle cone forebody could not be obtained with the usual no-smoothing NIC method. The axial flow solution given by the present method is presented in Fig. 8a. One hundred nodes were used with 35 of them on the forebody. The best value of γ_1 was found to be 0.01. Note again that the normal velocity errors are largest at the shoulders. A comparison of model and computed surfaces is given in Fig. 8b. Rounding of the shoulders and slight undulations are apparent. Experimental and computed pressures along a meridian for $\alpha = 0$ are given in Fig. 8c. As shown above, the rounding of the shoulders prevents simulation of the peak suction pressure, although the pressure gradients are captured satisfactorily.

Blunted 15-deg Cone Cylinders

Spherically blunted forebodies are often of interest for missile applications. However, good NIC solutions for such bodies are sometimes impossible to obtain because of the very large pressure gradients over the spherical cap. In this section, NIC results with smoothing are compared with data for 25% and 50% blunted 15-deg half-angle cone cylinders tested by Johnson.[30] One hundred nodes were used for each case with half of them on the forebody. For both cases, best results were obtained with $\rho = 1.05$ on the forebody and $\gamma_1 = 0.001$ and $\gamma_2 = 0.1$. Nodes on the cylinder were evenly spaced. The best nose tip inset distance was found to be one half of the radius of the spherical nose cap. Comparisons of computed results and experimental data for $\alpha = 0$ deg and for the windward and leeward meridians for $\alpha = 20$ deg are given in Figs. 9 and 10 for the 25 and 50% bluntness cases respectively. The comparisons are good except for the usual problem at the shoulder. The solutions, of course, do not reflect the effects of flow separation at the shoulder. Note that the better agreement for the 50% bluntness case at the shoulder is illusory. The data for the pressure tap at the shoulder were not reported.

For the ratio of angle of attack to cone half angle presented here (4/3), it would be expected that mild crossflow separation

would be encountered. However, as pointed out by Chu et al.,[31] the blunted noses and choice of the windward and leeward meridians for data/theory pressure comparisons minimizes the impact of the separated flow. (Johnson[30] does not present data for other azimuthal locations for the bodies considered here.)

Conclusions

It has been demonstrated that the usefulness of the NIC axial singularity method for representing inviscid, incompressible flow over inclined axisymmetric bodies can be dramatically extended by using a simple smoothing algorithm. The smoothing algorithm requires very little extra computational work and can easily be retrofitted to existing codes.

Copies of the interactive codes used in the present work can be obtained from the author.

Acknowledgment

The work reported in this paper was supported by the Transonic Aerodynamics Branch of NASA Langley Research Center under Contract NAS1-18000. Helpful discussions with M. R. Mendenhall of Nielsen Engineering & Research, Inc., are gratefully acknowledged.

References

[1]Von Kármán, T., "Calculation of Pressure Distribution on Airship Hulls," *Abhand. Aero. Inst. Tech. Hoch. Aachen,* No. 6, 3, 1927; (translated by D. Miner, NACA TM 574, 1930.

[2]Geer, J., and Anderson, C., "A Hybrid Perturbation Galerkin Technique with Applications to Slender Body Theory," NASA CR 178354, Aug. 1987; also ICASE Rept. No. 87-55.

[3]Thwaites, B., *Incompressible Aerodynamics,* Oxford, Clarendon Press, 1960.

[4]Moran, J. P., "Line Source Distributions and Slender-Body Theory," *Journal of Fluid Mechanics,* Vol. 17, 1963, pp. 285–304.

[5]Handelsman, R. A., and Keller, J. B., "Axially Symmetric Potential Flow Around a Slender Body," *Journal of Fluid Mechanics,* Vol. 28, Pt. 1, 1967, pp. 131–147.

[6]Geer, J., "Uniform Asymptotic Solutions for Potential Flow About a Slender Body of Revolution," *Journal of Fluid Mechanics,* Vol. 67, Pt. 4, 1975, pp. 817–827.

[7]Wong, T.-C., Liu, C. H., and Geer, J., "Comparison of Uniform Perturbation and Numerical Solutions for Some Potential Flows Past Slender Bodies," *Computers & Fluids,* Vol. 13, No. 3, 1985, pp. 271–283.

[8]Kaplan, C., "Potential Flow About Elongated Bodies of Revolution," NACA Rept. 516, 1935.

[9]Landweber, L., "Potential Flow About Bodies of Revolution and Symmetric Two-Dimensional Forms," Iowa Institute of Hydraulic Research Rept., Iowa State Univ., Ames, IA, Dec. 1959.

[10]Zedan, M. F., and Dalton, C., "Potential Flow Around Axisymmetric Bodies: Direct and Inverse Problems," *AIAA Journal,* Vol. 16, No. 3, 1978, pp. 242–250.

[11]Zedan, M. F., and Dalton, C., "Higher Order Axial Singularity Distributions for Potential Flow About Bodies of Revolution," *Computer Methods in Applied Mechanics and Engineering,* Vol. 21, 1980, pp. 295–314.

[12]D'Sa, J. M., and Dalton, C., "Body of Revolution Comparisons for Axial- and Surface-Singularity Distributions," *Journal of Aircraft,* Vol. 23, No. 8, 1986, pp. 669–672.

[13]Shu, J.-Y., and Kuhlman, J. M., "Calculation of Potential Flow Past Non-Lifting Bodies at Angle of Attack Using Axial and Surface Singularity Methods," NASA CR 166058, Feb. 1983.

[14]Kuhlman, J. M., and Shu, J.-Y., "Potential Flow Past Axisymmetric Bodies at Angle of Attack," *Journal of Aircraft,* Vol. 21, No. 3, 1984, pp. 218–220.

[15]Kuhlman, J. M., "Comment on 'Body of Revolution Comparisons for Axial and Surface Singularity Distributions,'" *Journal of Aircraft,* Vol. 24, No. 7, 1987, pp. 478–479.

[16]Oberkampf, W. L., and Watson, L. E., Jr., "Incompressible Potential Flow Solutions for Arbitrary Bodies of Revolution," *AIAA Journal,* Vol. 12, No. 3, 1974, pp. 409–411.

[17]Wolfe, W. P., and Oberkampf, W. L., "A Design Method for the Flow Field and Drag of Bodies of Revolution in Incompressible Flow," AIAA Paper 82-1359, Aug. 1982.

[18]Wolfe, W. P., and Oberkampf, W. L., "Drag Prediction for Projectiles and Finned Bodies in Incompressible Flow," AIAA Paper 85-0104, Jan. 1985.

[19]Campbell, G. S., "A Comparison of Methods for Calculating Flow about Irregular Bodies," *Simulation,* Vol. 37, Sept. 1981, pp. 92–98.

[20]Campbell, G. S., "Calculation of Potential Flow Past Simple Bodies Using Axial Sources and a Least Squares Method," *Journal of Aircraft,* Vol. 21, No. 6, 1984, pp. 437–438.

[21]Christopher, P. A. T., and Shaw, C. T., "Generation of Axi-Symmetric Body Shapes in Subsonic Flow by Means of Polynomial Distributions of Sources and Doublets Along the Axis of Symmetry," *Aeronautical Journal,* April 1987, pp. 155–169.

[22]Jones, D. J., "On the Representation of Axisymmetric Bodies at Zero Angles of Attack by Sources Along the Axis," *Canadian Aeronautics and Space Journal,* Vol. 27, No. 2, 1981, pp. 135–143.

[23]Janikowsky, L. C., and Sarpkaya, T., "Optimized Discrete-Singularity Representation of Axisymmetric Bodies," AIAA Paper 85-0284, Jan. 1985.

[24]Mendenhall, M. R., and Perkins, S. C., Jr., "Vortex Cloud Model for Body Vortex Shedding and Tracking," *Progress in Astronautics and Aeronautics: Tactical Missile Aerodynamics,* Vol. 104, edited by M. J. Hemsch and J. N. Nielsen, AIAA, New York, 1986, Chap. 12.

[25]Phillips, D. L., "A Technique for the Numerical Solution of Certain Integral Equations of the First Kind," *Journal of the Association for Computing Machines,* Vol. 9, 1962, pp. 84–97.

[26]Twomey, S., "On the Numerical Solution of Fredholm Integral Equations of the First Kind by the Inversion of the Linear System Produced by Quadrature," *Journal of the Association for Computing Machines,* Vol. 10, 1963, pp. 97–101.

[27]Lotz, I., "Calculation of Potential Flow Past Airship Bodies in Yaw," *Ingenieur-Archiv,* Vol. II, 1931, pp. 507-527 (translated in NACA TM 675, July 1932.)

[28]Dahlquist, G., and Björck, A., *Numerical Methods,* Prentice-Hall, Englewood Cliffs, NJ, 1974.

[29]Fox, C. H., Jr., "Experimental Surface Pressure Distributions for a Family of Axisymmetric Bodies at Subsonic Speeds," NASA TM X-2439, Dec. 1971.

[30]Johnson, W. E., "Experimental Investigation and Correlation with Theory of the Surface Pressure Distribution of Several Sharp and Blunted Cones for Incompressible Flow," MS Thesis, Univ. of Washington, Seattle, WA, 1963.

[31]Chu, J., Hall, R. M., and Kjelgaard, S. O., "Low-Speed Vortical Flow over a 5-Degree Cone with Tip Geometry Variations," Society of Automotive Engineers Paper 881422, Oct. 1988.